PCCP

Two-dimensional (P/T) studies of secondary/tertiary conformational dynamics in nucleic acids: Pressure induced melting and Maxwell Relations at the single molecule level

Journal:	*Physical Chemistry Chemical Physics*
Manuscript ID	CP-ART-12-2024-004664.R1
Article Type:	Paper
Date Submitted by the Author:	27-Jan-2025
Complete List of Authors:	Sung, Hsuan-Lei; University of Colorado, Department of Chemistry and Biochemistry Nesbitt, David; University of Colorado, Department of Chemistry and Biochemistry

Two-dimensional (P/T) studies of secondary/tertiary conformational dynamics in nucleic acids: Pressure induced melting and Maxwell Relations at the single molecule level

[1,2]Hsuan-Lei Sung and [1,2,3]David J. Nesbitt*

[1]JILA, National Institute of Standards and Technology and University of Colorado, Boulder, CO 80309, USA,

[2]Department of Chemistry, University of Colorado, Boulder, CO 80309, USA

[3]Department of Physics, University of Colorado, Boulder, CO 80309, USA

11/15/2024

*Email: djn@jila.colorado.edu

ABSTRACT

A predictive understanding of conformational folding of nucleic acids depends crucially on the underlying competition between enthalpic and entropic contributions to overall free energy changes. In extreme environments (e.g. deep ocean vents), such free energy changes are in turn impacted by both pressure and temperature as strongly coupled intensive variables, emphasizing the importance of a detailed molecular level understanding of the underlying thermodynamics. In this work, single-molecule fluorescence energy resonance transfer (smFRET) microscopy methods are implemented for quantitative study of secondary structure (i.e., DNA hybridization) and tertiary structure (i.e., RNA Mn^{2+} riboswitch folding) equilibria as a function of both pressure (P = 1 to 1000 bar) and temperature (T = 21 to 27 ℃). Temperature dependent studies at a series of fixed pressures reveal the single molecule DNA and RNA constructs to be stabilized and destabilized, respectively, with increasing T. Interestingly, results for the Mn^{2+} riboswitch indicate a positive entropy change ($\Delta S > 0$) for achieving the native tertiary conformation at all external pressures. This is contrary to more common physical expectations of increased order and thus an entropically penalty for tertiary

folding of the RNA. On the other hand, pressure dependent scans for a series of constant temperature conditions confirm that both the DNA hairpin and RNA riboswitch constructs destabilize ("melt") under increasing pressure, which by van't Hoff analysis implies a positive volume change ($\Delta V^0 > 0$) for both secondary and tertiary folding into the native state. Furthermore, slices through these two-dimensional free energy surfaces permit parameters for isobaric thermal expansion in both secondary and tertiary conformational folding coordinates to be extracted. Finally, experimental control of both (P, T) allows determination of the folding free energies as a two-dimensional function of pressure and temperature ($\Delta G(P, T)$). To the best of our knowledge, this facilitates a novel experimental confirmation of the underlying Maxwell relation $(\partial \Delta S/\partial P)_T = -(\partial \Delta V/\partial T)_P$ for the exact free energy differential $dG(P, V, S, T)$ at the single molecule level.

I. INTRODUCTION

Biological function in the cell is exquisitely impacted by 3D conformation of biomolecular structures,[1] which in turn can be modulated by an array of external thermodynamic variables[2] such as pressure and temperature in the intracellular environment. To understand how organisms manage and adapt to external pressure/temperature fluctuations, detailed characterization of the structural response of a biomolecule to such thermodynamic forces becomes crucially important.[3-5] Indeed, the quest for understanding these thermodynamic and kinetic impacts on biomolecular structure is further intensified by interest in the origin of life under extremophilic conditions, for example in deep-sea or potentially even extraterrestrial environments.[6-7]

Temperature is arguably the most commonly studied intensive thermodynamic variable, as it profoundly impacts biological function of organisms though diurnal and annual

thermal fluctuations in cellular surroundings. With notable exceptions,[8] most complex biomolecules (e.g. , proteins, enzymes, DNA, RNA nucleic acids) lose their native structure at elevated temperatures, i.e., denaturing with sufficient heating.[9] Such behavior is of course thermodynamically consistent with the simple physical picture that the *unfolded* biomolecular conformations are less ordered ($\Delta S^0 > 0$), and therefore entropically favored toward *unfolding* with increasing temperature.[10] Though far less well studied, the effects of pressure can be equally profound for biological structures, particularly for marine organisms where ambient pressures increase by 1 atm every 10 meters of depth and reach well into the kilobar range (1 kbar ≈ 1000 atm) in the deepest regions of the ocean.[11] As many species of marine life have evolved to survive at great ocean depths (e.g., in hot hydrothermal vents),[12-13] it is clearly of fundamental relevance to understand the coupling of temperature and pressure dependent effects on the structure and thermodynamic stability of biomolecules.[14]

Of particular interest, many complex biomolecules such as proteins and nucleic acids have been found to unfold ("melt") under increasing pressure.[15-16] The physical reasons behind such pressure induced unfolding ("denaturation") phenomena are not well understood and still remain a controversial topic.[8] Partially fueling this controversy is that such a result, at least initially, seems counterintuitive. Simple thermodynamic reversible work ($P\Delta V$) considerations predict pressure to favor the "maximally compact" conformations ($\Delta V < 0$) lowest free energy, which for nucleic acids might have been anticipated to be the form with greater secondary and/or tertiary structure. Although such a pressure induced melting phenomenon remains incompletely understood, one plausible explanation has been that the folded nucleic acid structure forms solvent-excluded "voids" and/or changes the hydration shell structure of the solvent, such that the *total* system volume (i.e., solute + solvent) is larger in the folded vs. unfolded state.[17-18] However, the volume changes for such processes can be quite small, providing additional challenges to any quantitative description of such phenomena. It is

therefore important to consider impacts from multiple competing microscopic hydration effects upon folding, between solute-solute (e.g. protein and/or nucleic acids), solvent-solvent, and solute -solvent hydration effects, relatively small differences in which could accentuate/reverse the net impact on pressure induced denaturation of biomolecules.[1, 19]

As a result of high levels of both biological relevance and interest, pressure-dependent conformational dynamics of proteins and nucleic acid biomolecules have been studied by multiple spectroscopic methods.[20-22] Due to simple mechanical limitations, this often has required minimizing sample size to reduce bulk volume and contact surface area, and thereby limiting the forces exerted by high external pressure.[23-24] Single molecule microscopy approaches offer the intrinsic advantage of relatively small sample size (in both volume and concentration) and have been utilized for high pressure experiments over the last decade (Fig. 1A).[16, 25] Furthermore, single molecule Fluorescence Resonance Energy Transfer (smFRET) methods bring additional advantages to such high pressure studies, whereby the energy transfer efficiency between donor/acceptor fluorophores offers quantitative structural information with which to identify a specific (e.g., folded/unfolded, hybridized/dehybridized) conformational state.[16, 26-27] Indeed, high pressure smFRET studies have proven quite informative in several nucleic acid systems, specifically demonstrating that single nucleic acid structures dehybridize ("melt") at modest (≈ 1 kbar) pressures, based on both equilibrium and kinetic measurements of the underlying pressure-dependent thermodynamics.[28-29] Interestingly, however, we are aware of no single molecule studies to date that have simultaneously been able to probe *both* the temperature and pressure dependence of RNA tertiary conformational dynamics,[30] the combination of which is essential to deconstructing pressure dependent free energies into enthalpic and entropic contributions.

The organization of this paper is as follows. In Section II we describe the experimental apparatus for pressure and temperature dependent single molecule folding, followed in Section

III by the equilibrium folding results. Specifically, Section IIIA addresses pressure dependent equilibrium thermodynamics, focusing on a 40A DNA hairpin as a simple model for free volume changes (ΔV^0) associated with secondary structure folding. In Section IIIB, we then utilize microscope stage heating methods to explore the temperature dependence of free volume (ΔV^0) changes in the well-studied 40A hairpin, which allows us to deconstruct the free energies (ΔG^0) and into entropic (ΔS^0) and enthalpic (ΔH^0) components for a more complete thermodynamic overview of the folding events. In Section IIIC, we extend these pressure and temperature dependent results for DNA structure formation to the RNA Mn^{2+} riboswitch, in order to explore and compare simple models for secondary vs. tertiary folding. In Section IV, these pressure and temperature dependent smFRET results are then interpreted to extract and elucidate the underlying thermodynamics of nucleic acid folding. Of particular interest, the free energy landscapes for these model DNA and RNA systems are found to depend quite differently on temperature, revealing starkly contrasting enthalpic and entropic advantages vs. penalties for secondary vs tertiary folding. Also, the novel availability of such thermodynamic data as a simultaneous function of both P and T allows extraction of cross derivatives such as single molecule thermal expansion coefficients ($(\partial\Delta V/\partial T)_P$) as well as the dependence of entropy change on pressure $(\partial\Delta S/\partial P)_T$, which by the properties of an exact differential (dG(P, V ,S, T)) must be rigorously interconnected. As a parting contribution, therefore, we analyze the smFRET data in light of these mathematical connections, which allow explicit empirical validation of the relevant Maxwell relation (i.e., $(\partial\Delta S/\partial P)_T = -(\partial\Delta V/\partial T)_P$) at the single molecule level.

II. EXPERIMENT

IIA. smFRET Sample preparation

The oligomer sequences and details of construct assembly for both the DNA 40A hairpin and RNA manganese riboswitch nucleic acid structures (Fig. 1B), have been discussed and presented in single molecule studies from our group. For simplicity, we therefore focus on specific modifications to the protocol relevant to the present study and refer the interested reader to previous work.[31-32]. Prior to each smFRET experiment, the nucleic acid constructs are diluted to ≈ 100 pM with imaging buffer to ensure sufficiently extended photobleaching lifetimes for fluorescence observation. The hemisodium HEPES imaging buffer (pH = 7.5) also contains the TROLOX/PCD/PCA oxygen scavenger system, background monovalent cations 100 mM KCl, and additional 0.5 mM $MgCl_2$ to facilitate the riboswitch folding. It has been previously demonstrated that submillimolar levels of Mg^{2+} are sufficient to promote loop-loop contact and successful tertiary folding of the manganese riboswitch, even in the complete absence ($[Mn^{2+}] = 0$) of the cognate Mn^{2+} ligand.[32] Most importantly, this allows us to focus on the Mg^{2+}-mediated tertiary structure formation dynamics. This is critical for achieving success in this study, since Mn^{2+} is also found to decrease the photostability of cyanine dyes,[33] which, with millisecond resolution/exposure times and the relatively high (50 μW) laser excitation conditions required for burst fluorescence methods, would otherwise be susceptible to severe photobleaching.

The sample holder is crafted from a hollow square capillary tube with a 75 μm × 75 μm internal square cross section to minimize optical aberration (Fig. 1A, right panel).[16, 34]Use of such a minimal surface area greatly decreases the net pressure-induced forces on the capillary walls, enabling us to routinely sustain pressures up to and in excess of 2 kilobars prior to failure. The outside of the capillary is coated with a polymer, which can be cleaned in a cool oxidizing flame to open a ≈ 1-inch-wide clear window and permit confocal laser access to the sample region via a water immersion microscope objective. We then flow in imaging buffer with fluorescently labelled (Cy3/Cy5) DNA or RNA (100 pM) constructs to achieve sufficiently

low densities of single molecule fluorophores in the confocal laser volume. The capillary end is then sealed and annealed with an oxygen/propane torch comfortably far (> 4") from the sample detection region, with the other capillary end sealed with epoxy into a narrow bore stainless high-pressure ferrule. Finally, the remaining open end of the fiber is dipped in silicon oil to form a freely translating/pressure transmitting membrane between the aqueous buffer and ethanol pressure reservoir, which can be manually varied from 1 to 5000 bar by a piston driven hydraulic system and measured with a high-pressure manometer.

IIB. High pressure smFRET experiment and data analysis

To achieve high pressure operating conditions, a manual piston (Fig. 1A) supplies up to 5 kbar to a stainless-steel tubing manifold filled with ethanol as the pressure transmitting fluid. Prior to each single molecule experiment, the sample holder, capillary and ferrule assembly is mounted onto a high-pressure valve via an optical rail system to allow positioning with respect to the surface and optical axis of the microscope objective. Once the rectangular window of the sample is correctly translated (xyz) and rotated (ϕ) with respect to the objective axis, the entire capillary is raised to the desired pressure by the piston pump.

The smFRET experiment is performed with a home-built confocal microscope system with alternating (two color, green/red) laser excitation (ALEX) to ensure the presence of both donor and acceptor species on a given construct. In brief, the 532 nm and 633 nm pulsed lasers (20 MHz repetition rate) are first collimated and then focused into the sample with a high numerical aperture (NA = 1.2) water immersion objective.[35] The resulting photon stream emitted through the glass capillary walls is subsequently recollimated with the same epifluorescence objective, sorted by color/polarization, and imaged onto avalanche photodiode (APD) single photon counting detectors. For each photon event, we record the i) color (red vs.

green), ii) polarization (horizontal vs. vertical), iii) "micro-time" with time-to-amplitude converters (achieving ≈ 50 ps precision) with respect to the laser pulse, and iv) "macro-time" i.e. wall-clock time (with ≈ 50 ns precision) for postprocessing of the single molecule diffusion dynamics. From the micro-time information, we obtain relative count rates of red (I_R) vs green (I_G) fluorescence photons associated with 532 nm excitation, while the presence of additional red photon emission from purely 633 nm pulsed excitation confirms that the freely diffusing single molecule constructs contain both Cy3 and Cy5 fluorophore labels.[36]

In such "burst fluorescence" smFRET experiments, the fluorescent constructs are untethered to the capillary wall surface and allowed to freely diffuse through the laser beam. The fluorescence events are thus only observed when a single construct diffuses through the confocal volume, and for each event ("burst") the photon rates (red vs. green) are used to estimate the FRET efficiency for a single freely diffusing encounter. With information collected from thousands of such single molecule burst events, we can then calculate the E_{FRET} probability distribution from $E_{FRET} = I_R/(I_R+I_G)$. As shown in sample data in Fig. 2A, the DNA construct clearly reveals two well-resolved FRET subpopulations, the distributions of which are least squares fit to a sum of two Gaussians. The folding equilibrium constant (K_{fold}) for both DNA and RNA constructs can then be calculated from the ratio of the folded (high E_{FRET}) to the unfolded (low E_{FRET}) populations obtained from the integrated Gaussian areas.

IIC. Sample temperature control

In order to explore temperature dependence of these high pressure experiments (or equivalently, pressure dependence of these temperature dependent studies), the temperature of the capillary varied under servo-loop control by resistive heaters mounted onto the microscope objective,[37] incorporating a sample cover to minimize ambient air currents and thermal drift.

Prior to any data acquisition, the system is allowed to equilibrate for 30 minutes to achieve reliable, steady state thermalization, with both temperature and temperature fluctuations monitored throughout the experiment. The fluctuations are observed to be ≈ 0.2 °C, i.e., significantly smaller than the 2.5 °C grid of temperature intervals explored in these studies. We note that dissociation constant of water is weakly temperature dependent, and so is the pH value of our aqueous sample solution. However, the pH variation is estimated to be < 0.1 within our temperature range for our HEPES buffer and does not significantly affect the conformation of the smFRET constructs.

III. RESULTS

IIIA. 40A hairpin DNA secondary structures destabilize with *increasing* pressure

The 40A DNA hairpin construct serves as a well-studied model system to investigate the stability of nucleic acid secondary structure under external thermodynamic pressure and temperature perturbations.[31] The two complementary strands are each labeled with Cy3 and Cy5 respectively and separated by a 40-adenine loop with 8 complementary base pairs in the stem region (5'-ACTGAAGA-$(A)_{40}$-TCTTCAGT-3').[27] As the DNA hairpin folds and forms the stem-loop structure through Watson–Crick base pairing, the fluorophore distance decreases systematically and enhances FRET energy transfer. We thus anticipate unfolded/folded conformations to reveal themselves as low/high E_{FRET} states, respectively. Indeed, the 40A DNA hairpin shows two clearly resolved populations in the FRET histograms (see Fig. 2A), consistent with these expectations.

Under ambient pressure conditions (P ≈ 1 bar), the FRET distributions exhibit approximately equal populations for folded and unfolded 40A DNA hairpin conformations (Fig. 2A). As a function of increasing hydrostatic pressure (1 to 750 bar, T = 26.8 °C), however,

the high/low E_{FRET} populations systematically decrease/increase respectively, which reflects the DNA hairpin stem dehybridizing ("melting") from folded to unfolded conformation. Such "pressure-induced denaturation" effects have been noted for both protein and nucleic acid structures and previously reported in the literature,[15] with the unique capabilities of the current apparatus further permitting us to examine such phenomena from a i) dual pressure/temperature dependent and ii) single molecule thermodynamic perspectives. For the moment, we note from Fig. 2A and the simple equilibrium relation

$$\Delta G^0 = -P(\Delta V^0) = -RT\ln(K_{fold}) \qquad \text{(Eq. 1)}$$

that such a spontaneous pressure-induced denaturation unambiguously implies an *increase* in free volume ($\Delta V^0 > 0$) upon secondary structure formation of the 40A DNA Hairpin stem under isothermal conditions. More quantitatively, Eq. 1 permits extraction of the isothermal change in free volume from a plot of $\ln(K_{fold})$ vs P (see Fig. 2B), the slope of which yields ΔV = 17.8(0.4) mL/mol at 26.8 ℃. It is worth stressing that the magnitude of such free volume changes upon hybridization is roughly equivalent to a single water molecule (18 mL/mol), clearly representing only an exceedingly small fraction of the overall DNA construct volume. Irrespective of absolute magnitude, however, the sign of this pressure dependent free volume change is singularly impactful. This predicts, for example, a pressure induced destabilization of dsDNA for marine life at the bottom of the ocean and in deep sea vents.[12-13]

IIIB. *Increasing* temperature *destabilizes secondary structure* in the 40A DNA hairpin

In the temperature dependent experiments for freely diffusing constructs under variable pressure conditions (see Fig. 3A), the equilibrium constant for folding of the 40A DNA hairpin exhibits a rapid exponential decrease with increasing pressure. However, temperature has an equally significant impact on the equilibrium structure of DNA, resulting in dehybridization

("melting") of secondary Watson-Crick base pair structure. Upon closer examination of the data in Fig. 3A, one can furthermore see that the intercepts and pressure dependent slopes change visibly even over the relatively modest range ($\Delta T \approx 6$ C) of temperatures sampled experimentally. Most importantly, this indicates that increasing temperature not only dramatically lowers the equilibrium constant for DNA 8 bp stem hybridization under constant pressure conditions, but also that such temperature sensitivities are additionally dependent on applied external pressure. In simplest thermodynamic terms, this implies that the free volume change ($\Delta V^0(T)$) for secondary structure folding of the 40A hairpin DNA is itself a function of temperature (e.g., thermal expansion or contraction), a point we will address in the discussion section. Specifically, we note that Fig. 3B indicates a significant temperature dependent impact on the free volume change (ΔV) for folding (from $\Delta V \approx 24.7(1.4)$ to $17.8(0.4)$ mL/mol, see Table I), which allows novel empirical extraction of partial derivatives of ΔV and ΔS with respect to the corresponding conjugate variables P and T. We will explicitly return to this later in the discussion, but simply note for now that such cross partial derivative capabilities permit empirical tests and confirmations of the Maxwell relations between $(\partial\Delta V/\partial T)_P$ and $(\partial\Delta S/\partial P)_T$ at the single molecule level.

IIIC. *Increasing* pressure *destabilizes tertiary folding* of the RNA Mn^{2+} riboswitch

It is of equivalent biophysical value to probe the thermodynamic response for *ribonucleic acid* (RNA) construct folding as a function of external pressure and temperature. Of particular relevance to these folding studies, RNA naturally occurs as a single stranded species and is able to form both secondary and tertiary structures. Interestingly, previous pressure/temperature efforts have focused on secondary structure in nucleic acids, largely ignoring potential thermodynamic impacts on any corresponding changes in tertiary conformation.[16, 38-39] To address this issue, we have therefore chosen to also explore tertiary folding dynamics for the RNA Mn^{2+} riboswitch, as a model RNA system for probe/compare

pressure/temperature dependent changes in *tertiary* vs. *secondary* nucleic acid structures.[40] Riboswitches are RNA motifs upstream of the genomic mRNA which undergo tertiary conformational transitions that translationally or transcriptionally regulate gene expression by sensing the presence/absence of cognate ligands in the cellular environment.[41] The structure of the Mn^{2+} riboswitch construct is identical to that used in previously single molecule work.[29, 32, 42] Importantly, this also permits taking advantage of a thoroughly tested smFRET construct design used in previous investigations of temperature dependent single molecule folding kinetics as a function of both Mg^{2+} and Mn^{2+} divalent species. Indeed, to achieve maximum cationic simplicity in the folding behavior, we choose to work in the absence of the cognate ligand Mn^{2+}, which allows us to isolate and highlight the purely Mg^{2+}-promoted loop-loop tertiary interaction thermodynamics previously determined to be important in this riboswitch.[32]

To complement the above DNA results described in Sec. IIIA, B, we therefore have explored burst fluorescence studies under isothermal conditions for freely diffusing RNA riboswitch constructs, varying external pressures in the capillary samples from 1 bar to 500 bar. As noted above for secondary structure formation in the 40A DNA hairpin, the FRET histograms (see data in Fig 4A) reveal an even larger systematic *decrease* in K_{fold} (i.e., *destabilization* of riboswitch structure) with increasing pressure, predicting *even larger increases* in free volume upon RNA tertiary structure formation. More quantitatively, the slope from the corresponding van't Hoff plot in Fig. 4A indicates a $\Delta V = 71(9)$ mL/mol change in free volume (at 26.6 ^{o}C) upon folding (Table II). Tertiary structure sensitivity to external pressure for the RNA manganese riboswitch is therefore substantially (3-4x) stronger than observed for secondary structure formation in the simple 8 bp 40 A hairpin DNA construct.

IIID. *Increasing* temperature *stabilizes tertiary folding* of the RNA Mn^{2+} riboswitch

Continuing this parallel comparison of DNA/RNA nucleic acid constructs, we next explore the corresponding temperature dependence of free volume changes for the RNA Mn^{2+} riboswitch tertiary structure. Indeed, inspection of the pressure/temperature dependent data in Fig. 4A reveals that the van't Hoff plots for K_{fold} all shift systematically to *higher* values as a function of *increasing* temperature. Stated alternatively, *decreasing* temperature *destabilizes* tertiary structure in the Mn^{2+} riboswitch construct. This represents a relatively novel example of "cold denaturation" of nucleic acids, with relatively few such cases reported in the literature.[42-44] This differs fundamentally from the more conventional behavior observed for the 40 A hairpin DNA (see Fig. 3A), which clearly exhibits a more typical *destabilization* of secondary structure (i.e., "heat denaturation") with *increasing* temperature. Previous work has suggested that such novel "cold denaturation" phenomena in RNA constructs might reflect an exceptional case, due to the presence of purely Mg^{2+} promoted folding pathway in the absence of the cognate riboswitch Mn^{2+} ligand.[42] Further pressure and temperature dependent folding studies as a function of both Mn^{2+} and Mg^{2+} cation concentrations will be necessary to confirm or reject such an interpretation. For the present purposes, however, such unambiguous sign differences in the temperature dependence for the DNA vs RNA single molecule constructs offers greater behavioral diversity in our comparison/interpretation of the secondary and tertiary folding thermodynamics.

As a final comment on the Mn^{2+} riboswitch data, the nearly parallel slopes in Fig. 4A indicate "cold denaturation" behavior for RNA tertiary structure to be only very weakly dependent on pressure. This is in stark contrast with the DNA hairpin studies (Fig. 3A), for which there is a pronounced *decrease* in slope with increasing temperature. This is additionally evident by inspection of the corresponding free volume changes in Fig. 4B, which demonstrates a slow but finite drop in $\Delta V(T)$ as a function of increasing temperature. It is particularly interesting to note that, despite these dramatic sign differences in ΔH and ΔS (e.g., resulting in

hot vs cold denaturation behavior) between the 40A Hairpin and RNA Mn^{2+} riboswitch, the qualitative shapes of $\Delta V(T)$ vs T curves are similar for both constructs (Fig. 3B, 4B). A self-consistent interpretation would be that the negative slopes in both $\Delta V(T)$ vs T plots (Fig. 3B, 4B) imply a *weakening* of the pressure dependent *destabilization* (i.e., decrease in ΔV) for both DNA (secondary) and RNA (tertiary) folding with *increasing* temperature.

IIIV. Synergistic P/T effects on secondary and tertiary folding thermodynamics

Two-dimensional pressure and temperature dependent studies provide particularly valuable information on coupled thermodynamic interactions between thermodynamic conjugate variable pairs, e.g., V and P.[27] Indeed, results from Sec IIIA to D have explicitly focused on pressure-volume contributions ($P\Delta V(T)$) to the folding free energy landscape, providing detailed characterization for each of the DNA and RNA nucleic acid constructs. Here we briefly note that the data also contains complementary information on yet another conjugate variable pair, T and S. Specifically, the Van't Hoff temperature dependence of $\ln(K_{fold})$ in Figs. 5A and 6A provides quantitative information on both the change in enthalpy (ΔH^0 from slopes) and entropy (ΔS^0 from intercepts) upon secondary and tertiary folding (see both Table III and IV). For the DNA hairpin, the experimentally observed negative entropy change ($\Delta S < 0$) value is consistent with conventional "heat denaturation" behavior, for which the free energy contribution to folding ($-T\Delta S$) becomes less favored (i.e., $\Delta\Delta G > 0$) with increasing temperature. Interestingly, however, the DNA hairpin (Fig. 5B) clearly demonstrates a *positive* growth in ΔS with respect to P. Since $\Delta S < 0$, this means ΔS becomes less negative with pressure, which in turn correctly predicts that increasing pressure reduces the temperature sensitivity (i.e., the slope of $-T\Delta S$ vs T) associated with "heat denaturation" and strongly

exothermic folding ($\Delta H < 0$). The relevant thermodynamic values extracted for the DNA hairpin (ΔH, ΔS) are summarized as a function of pressure in Table III.

Interestingly, however, the thermodynamic landscape changes considerably for RNA tertiary vs DNA secondary folding. Inspection of Fig. 6A and Table IV indicate tertiary structure formation in the RNA riboswitch construct to be entropically favored ($\Delta S > 0$). Consequently, folding is now thermodynamically favored with increasing temperature (i.e., $-T\Delta S < 0$), in agreement with "cold denaturation" behavior. We arrive at the same conclusion from the sign of enthalpy change ($\Delta H > 0$) indicated in Table IV upon tertiary structure formation, which implies by Le Chatelier's principle the need for increased temperature to enhance an endothermic folding process. Fig. 6B and Table IV reveal that ΔS values for the RNA riboswitch construct nevertheless *increase* with pressure. Thus, even despite opposing signs for (ΔS, ΔH) upon folding and a complete reversal of these signs between DNA and RNA constructs, such an increase in ΔS with pressure is in fact qualitatively similar to that of the DNA hairpin (see Fig. 5B and 6B). Simply summarized, this implies that increasing pressure enhances the thermal sensitivity (i.e, $-T\Delta S < 0$ negative contributions to ΔG) for both nucleic acid constructs. This is completely consistent with the experimental observation of pressure-induced "melting" of both secondary (DNA) and tertiary (RNA) nucleic acid constructs at high pressures.

IV. DISCUSSION

IVA: Pressure denaturation from the full suite of thermodynamic characterization

The data clearly reveal that both secondary (DNA hairpin) and tertiary (RNA riboswitch) structures unfold at high pressures. This is consistent with previous reports that many biomolecules lose their native structures with increasing pressure.[15] Such pressure denaturation

behavior for proteins has been well known for decades and unambiguously implies a positive volume change ($\Delta V > 0$) upon folding.[45] It is this combination of increasing free volume while achieving a more ordered structure that at first seems counterintuitive. However, such a volume increase accompanying greater structure is in principle captured by simple physical models whereby water-excluding cavities are formed upon folding of hydrophobic motifs in the protein.[17-18] However, the proposed notion of small "hydrophobic cavities" in proteins would suggest such volume changes to be less pronounced for nucleic acids,[46] particularly DNA hybridization, where a well-characterized secondary structure is formed via hydrogen bonding between Watson-Crick base pairs.[47] Nevertheless, pioneering work on DNA melting in the 1990s did demonstrate the thermal stability of dsDNA to significantly depend on external pressure,[39, 48] despite the lack of crystallographic evidence for any such "hydrophobic cavities" in the DNA double helix structure. Indeed, as more advanced molecular dynamics simulations have succeeded in explicitly including water-biomolecule interactions,[49] a different hydration model paradigm seems to be emerging that invokes significant reorganization of solvent water molecules around a secondary or tertiary structure forming region. Though more work will be required to confirm/reject such a model, reorganization of the surrounding water molecule network offers a powerful and potentially more intuitive physical picture with which to explain the small but positive free volume changes ($\Delta V > 0$) experimentally observed upon nucleic acid folding.

Specifically, this alternative "hydration model" recognizes the crucial importance of the overall sum of "solvent + solute" volume changes for the nucleic acid + water system.[1] In general, greater hydration results in a more ordered and compact water structure due to Coulombic attraction and thus would tend to predict a decrease in total volume.[50] Upon nucleic acid folding, however, cation association/neutralization and reduction in solvent-exposed surface area result in a weaker hydration shell,[51] leading to an increase in folded state volume

($\Delta V > 0$) and thus correctly predicting pressure-induced denaturation. Indeed, even the "hydrophobic cavity" models may have to be reinterpreted to reflect substantial changes in the surrounding water configuration.[17-18] Specifically, any such cavities formed by the folded biomolecule do not even require exclusion of water. Indeed, water molecules in such nanoscale confinement regions have been experimentally demonstrated to be less structured and therefore lower in density (i.e., $\Delta V > 0$) than the surrounding solvent.[52] Hence one could imagine "partially hydrated cavity" models as valuable directions to consider in theoretical modeling.

If folding induced reconfiguration of the surrounding solvent/water is largely responsible for the experimental observation of $\Delta V > 0$, it is perhaps not surprising that ΔV would also depend on temperature. Indeed, our pressure and temperature dependent studies clearly reveal (see Table I) that $\Delta V > 0$ systematically decreases with increasing temperature, irrespective of the secondary (DNA) vs. tertiary (RNA) structure of the construct explored and, for the present studies, even the positive vs. negative sign of ΔS. As one simple interpretation, water becomes increasingly less structured with increasing thermal energy, and therefore any volume differences between hydrating water, non-hydrating water, and nanoconfined water molecule would be expected to diminish with temperature, leading to a weaker pressure induced melting (i.e., less positive ΔV) response. Furthermore, it is important to note that in any of these alternative models, $\Delta V > 0$ arises predominantly from interaction of the biomolecule with the surrounding solvent network, and thus cannot be identified from crystallographic structure itself. Finally, we mention that these volume changes for nucleic acid folding have also been previously demonstrated to depend strongly depend on monovalent cation concentrations,[28] with a dramatic lowering of ΔV by nearly two-fold under physiological Na^+ conditions. This pronounced sensitivity to cationic environment further highlights the crucial importance of considering "solute + solvent" interactions in predicting and interpreting pressure-induced melting behavior in nucleic acids.

IVB. Maxwell relations and beyond conventional thermodynamic analysis

From conventional isothermal Van't Hoff analysis, the volume change ΔV is obtained from slope of the lnK vs P plot (Eq. 1). With temperature as additional independent variable, V(T) can be written to lowest order as

$$V^{f/u}(T) \approx V_0^{f/u}(1 + \alpha^{f/u}(T-T_{ref})), \quad \text{(Eq. 2)}$$

where $V_0(T)$ is the molar volume at the reference temperature and α is the thermal expansion coefficient. As a result, the volume change $\Delta V(T) = V^f(T)-V^u(T)$ between the folded and unfolded states should also depend linearly on temperature, as empirically verified in Figs. 3B and 4B. To elucidate the slopes of these linear dependences, we can further deconstruct ΔV(T) into folded and unfolded contributions

$$\Delta V(T) = [V_0^f (1 + \alpha^f(T-T_{ref})] - [V_0^u (1 + \alpha^u(T-T_{ref}))]$$

$$= (V_0^f - V_0^u) + (V_0^f\alpha^f - V_0^u\alpha^u) (T-T_{ref}), \quad \text{(Eq. 3)}$$

where $V_0^{f/u}$ and $\alpha^{f/u}$ correspond to V_0 and α for the folded/unfolded state, respectively. The slope in the ΔV vs T plots (Fig. 3B and 3D) is thus $V_0^f\alpha^f - V_0^u\alpha^u$, which is experimentally seen to be weakly negative for both secondary and tertiary nucleic acid folding. To achieve a negative slope requires $V_0^u\alpha^u > V_0^f\alpha^f$, which for $V_0^f > V_0^u$ implies $\alpha^u > \alpha^f$. Although more work is needed to establish this mechanism unambiguously, such behavior would be consistent with the simple physical picture of solvent waters accessing a more compact and locally ordered structure around the unfolded vs folded nucleic acid constructs as the dominant reason for achieving an increased free volume upon folding. This would also match the experimental observation ($\alpha^u > \alpha^f$) of a higher thermal expansion coefficient in unfolded vs folded species

due to thermal ejection of more highly ordered water molecules from the nucleic acid-water interface.

As a final comment, we can use the well-known mathematical properties of an exact differential (dG)

$$dG = \Delta E + P\Delta V + V\Delta P - T\Delta S - S\Delta T \qquad \text{(Eq. 4)}$$

to experimentally test the relationship between the two pairs of conjugate thermodynamic variables (P, V) and (T, S). Since partial derivatives commute for any analytic function, we can exploit this symmetry to yield

$$\left(\frac{\partial}{\partial P}\left(\frac{\partial \Delta G}{\partial T}\right)_P\right)_T = \left(\frac{\partial}{\partial T}\left(\frac{\partial \Delta G}{\partial P}\right)_T\right)_P. \qquad \text{(Eq. 5)}$$

By comparison of Eq 5 and 4, one immediately recognizes $(\partial\Delta G/\partial T)_P = \Delta S$ and $(\partial\Delta G/\partial P)_T = -\Delta V$, which can therefore be rewritten in the form of a rigorous Maxwell relation between S, T and P, V:

$$\left(\frac{\partial \Delta S}{\partial P}\right)_T = -\left(\frac{\partial \Delta V}{\partial T}\right)_P. \qquad \text{(Eq. 6)}$$

Eq. 6 makes a very simple prediction, which can be easily tested against our single molecule thermodynamic data. Specifically, the right-hand side of the Eq. 6 is equivalent to the slopes in a plot of ΔV vs T (see Fig. 3B and 4B), while the left-hand side is nicely captured by the corresponding slopes in Fig. 5B and 6B. Quantitatively, the left and right sides of Eq. 5 are found to be $(\partial\Delta S/\partial P)_T = 1.11(25)$ and $-(\partial\Delta V/\partial T)_P = 1.16(23)$ mL/mol/K, respectively, for the DNA hairpin construct. Similarly for tertiary structure in the RNA Mn^{2+} riboswitch, the corresponding two partial derivatives are $(\partial\Delta S/\partial P)_T = 1.40(24)$ vs $-(\partial\Delta V/\partial T)_P = 1.8(5)$ mL/mol/K. As summarized in Table V, both sets of results agree well with predictions from Eq 6 to within experimental uncertainty. It is worth noting that such Maxwell relations at the single molecule level provide novel strategies to measure thermodynamic quantities otherwise

quite difficult to measure.[53] For instance, Eq. 5 permits the more challenging quantity $(\partial\Delta S/\partial P)_T$ to be evaluated through simpler isobaric thermal expansion experiments. To the best of our knowledge, these results offer a novel first confirmation of the Maxwell relation between conjugate thermodynamic variables (S, P) and (V, T) with respect to Gibbs free energy at the single molecule level.

V. Summary and conclusion

The combination of high pressure and temperature control coupled with confocal-based single-molecule FRET microscopy has been used to successfully demonstrate detailed two-dimensional thermodynamic study of nucleic acid conformational dynamics at the single molecule level. First of all, the studies determine that both DNA (secondary) and RNA (tertiary) nucleic acid structures unfold with increasing pressure. This pressure induced denaturation necessarily signals an *increase* in total solute + solvent total free volume ($\Delta V > 0$) for nucleic acid folding, which we have attributed to weaker solvation/less highly ordered water molecules sampling the "solvent accessible surface area" (SASA) of the nucleic acid aqueous liquid interface. Moreover, this corresponding change in free volume (ΔV) is found to monotonically *decrease* with *increasing* temperature, suggesting that it is the presence of randomized solvating water molecules that shifts the equilibrium over to a folded conformation, with a simple physical picture in agreement with the unfolding induced change in thermal expansion ($\alpha^u > \alpha^f$) derived from the corresponding pressure-temperature studies. Finally, the current two-dimensional studies as a function of pressure (1 to 750 bar) and temperature (20 to 27°C) have provided first data with which to test and validate the fundamental Maxwell relation $(\partial\Delta S/\partial P)_T \approx -(\partial\Delta V/\partial T)_P$ for formation of both secondary (DNA hairpin) and tertiary (RNA Mn^{2+} riboswitch) nucleic acid structure at the single molecule level.

ACKNOWLEDGEMENTS

Initial support for this work has been through the National Science Foundation (CHE 2053117) from the Chemical, Structure, Dynamics and Mechanisms-A Program, with current support from the Air Force Office of Scientific Research (FA9550-15-1-0090) and additional funds for development of the high-pressure apparatus from PHY-2317149 (Physics Frontier Center Program). We would also like to acknowledge early seed contributions by the W. M. Keck Foundation Initiative in RNA Sciences at the University of Colorado, Boulder.

REFERENCES

1. van Gunsteren, W. F.; Luque, F. J.; Timms, D.; Torda, A. E., Molecular Mechanics in Biology: From Structure to Function, Taking Account of Solvation. *Annu. Rev. Biophys.* **1994,** *23* (Volume 23, 1994), 847-863.

2. Smeller, L., Pressure–Temperature Phase Diagrams of Biomolecules. *BBA - Protein struct. Mol. Enzymol.* **2002,** *1595* (1), 11-29.

3. Oger, P. M.; Jebbar, M., The Many Ways of Coping with Pressure. *Res. Microbiol.* **2010,** *161* (10), 799-809.

4. Sawle, L.; Ghosh, K., How Do Thermophilic Proteins and Proteomes Withstand High Temperature? *Biophys. J.* **2011,** *101* (1), 217-227.

5. Ando, N.; Barquera, B.; Bartlett, D. H.; Boyd, E.; Burnim, A. A.; Byer, A. S.; Colman, D.; Gillilan, R. E.; Gruebele, M.; Makhatadze, G., et al., The Molecular Basis for Life in Extreme Environments. *Annu. Rev. Biophys.* **2021,** *50* (Volume 50, 2021), 343-372.

6. Coleine, C.; Delgado-Baquerizo, M., Unearthing Terrestrial Extreme Microbiomes for Searching Terrestrial-Like Life in the Solar System. *Trends Microbiol.* **2022,** *30* (11), 1101-1115.

7. Noirungsee, N.; Changkhong, S.; Phinyo, K.; Suwannajak, C.; Tanakul, N.; Inwongwan, S., Genome-Scale Metabolic Modelling of Extremophiles and Its Applications in Astrobiological Environments. *Environ. Microbiol. Rep.* **2024,** *16* (1), e13231.

8. Silva, J. L.; Weber, G., Pressure Stability of Proteins. *Annu. Rev. Phys. Chem.* **1993,** *44*, 89-113.

9. Larson, B. L.; Rolleri, G. D., Heat Denaturation of the Specific Serum Proteins in Milk. *J. Dairy. Sci.* **1955,** *38* (4), 351-360.

10. Lazaridis, T.; Karplus, M., Heat Capacity and Compactness of Denatured Proteins. *Biophys. Chem.* **1999,** *78* (1), 207-217.

11. Kato, C.; Li, L.; Nogi, Y.; Nakamura, Y.; Tamaoka, J.; Horikoshi, K., Extremely Barophilic Bacteria Isolated from the Mariana Trench, Challenger Deep, at a Depth of 11,000 Meters. *Appl. Environ. Microbiol.* **1998,** *64* (4), 1510-1513.

12. Jannasch, H. W.; Wirsen, C. O.; Molyneaux, S. J.; Langworthy, T. A., Extremely Thermophilic Fermentative Archaebacteria of the Genus *Desulfurococcus* from Deep-Sea Hydrothermal Vents. *Appl. Environ. Microbiol.* **1988,** *54* (5), 1203-1209.

13. Miroshnichenko, M. L.; Bonch-Osmolovskaya, E. A., Recent Developments in the Thermophilic Microbiology of Deep-Sea Hydrothermal Vents. *Extremophiles* **2006,** *10* (2), 85-96.

14. Yayanos, A. A.; Dietz, A. S.; Van Boxtel, R., Obligately Barophilic Bacterium from the Mariana Trench. *Proc. Natl. Acad. Sci. U.S.A.* **1981,** *78* (8), 5212-5215.

15. Brandts, J. F.; Oliveira, R. J.; Westort, C., Thermodynamics of Protein Denaturation. Effect of Pressure on the Denaturation on Ribonuclease A. *Biochemistry* **1970,** *9* (4), 1038-1047.

16. Patra, S.; Anders, C.; Erwin, N.; Winter, R., Osmolyte Effects on the Conformational Dynamics of a DNA Hairpin at Ambient and Extreme Environmental Conditions. *Angew. Chem. Int. Ed.* **2017,** *56* (18), 5045-5049.

17. Roche, J.; Caro, J. A.; Norberto, D. R.; Barthe, P.; Roumestand, C.; Schlessman, J. L.; Garcia, A. E.; García-Moreno E., B.; Royer, C. A., Cavities Determine the Pressure Unfolding of Proteins. *Proc. Natl. Acad. Sci. U.S.A.* **2012,** *109* (18), 6945-6950.

18. Jenkins, K. A.; Fossat, M. J.; Zhang, S.; Rai, D. K.; Klein, S.; Gillilan, R.; White, Z.; Gerlich, G.; McCallum, S. A.; Winter, R., et al., The Consequences of Cavity Creation on the Folding Landscape of a Repeat Protein Depend upon Context. *Proc. Natl. Acad. Sci. U.S.A.* **2018,** *115* (35), E8153-E8161.

19. Harano, Y.; Kinoshita, M., Crucial Importance of Translational Entropy of Water in Pressure Denaturation of Proteins. *J. Chem. Phys.* **2006,** *125* (2).

20. Jonas, J.; Ballard, L.; Nash, D., High-Resolution, High-Pressure NMR Studies of Proteins. *Biophys. J.* **1998,** *75* (1), 445-452.

21. Schroer, M. A.; Paulus, M.; Jeworrek, C.; Krywka, C.; Schmacke, S.; Zhai, Y.; Wieland, D. C. F.; Sahle, C. J.; Chimenti, M.; Royer, C. A., et al., High-Pressure SAXS Study of Folded and Unfolded Ensembles of Proteins. *Biophys. J.* **2010,** *99* (10), 3430-3437.

22. Smeller, L., Biomolecules under Pressure: Phase Diagrams, Volume Changes, and High Pressure Spectroscopic Techniques. *Int. J. Mol. Sci.* **2022,** *23* (10), 5761.

23. Raber, E. C.; Dudley, J. A.; Salerno, M.; Urayama, P., Capillary-Based, High-Pressure Chamber for Fluorescence Microscopy Imaging. *Rev. Sci. Instrum.* **2006,** *77* (9).

24. Teixeira, S. C. M.; Leão, J. B.; Gagnon, C.; McHugh, M. A., High Pressure Cell for Bio-SANS Studies under Sub-Zero Temperatures or Heat Denaturing Conditions. *J. Neutron Res.* **2018,** *20*, 13-23.

25. Vass, H.; Lucas Black, S.; Flors, C.; Lloyd, D.; Bruce Ward, F.; Allen, R. J., Single-Molecule Imaging at High Hydrostatic Pressure. *Appl. Phys. Lett.* **2013,** *102* (15).

26. Patra, S.; Anders, C.; Schummel, P. H.; Winter, R., Antagonistic Effects of Natural Osmolyte Mixtures and Hydrostatic Pressure on the Conformational Dynamics of a DNA Hairpin Probed at the Single-Molecule Level. *Phys. Chem. Chem. Phys.* **2018,** *20* (19), 13159-13170.

27. Sung, H.-L.; Nesbitt, D. J., DNA Hairpin Hybridization under Extreme Pressures: A Single-Molecule FRET Study. *J. Phys. Chem. B* **2020,** *124* (1), 110-120.

28. Sung, H.-L.; Nesbitt, D. J., Single-Molecule Kinetic Studies of DNA Hybridization under Extreme Pressures. *Phys. Chem. Chem. Phys.* **2020,** *22* (41), 23491-23501.

29. Sung, H.-L.; Nesbitt, D. J., Ligand-Dependent Volumetric Characterization of Manganese Riboswitch Folding: A High-Pressure Single-Molecule Kinetic Study. *J. Phys. Chem. B* **2022,** *126* (47), 9781-9789.

30. Arns, L.; Knop, J.-M.; Patra, S.; Anders, C.; Winter, R., Single-Molecule Insights into the Temperature and Pressure Dependent Conformational Dynamics of Nucleic Acids in the Presence of Crowders and Osmolytes. *Biophys. Chem.* **2019,** *251*, 106190.

31. Nicholson, D. A.; Sengupta, A.; Sung, H.-L.; Nesbitt, D. J., Amino Acid Stabilization of Nucleic Acid Secondary Structure: Kinetic Insights from Single-Molecule Studies. *J. Phys. Chem. B* **2018,** *122* (43), 9869-9876.

32. Sung, H.-L.; Nesbitt, D. J., Single-Molecule FRET Kinetics of the Mn^{2+} Riboswitch: Evidence for Allosteric Mg^{2+} Control of "Induced-Fit" vs "Conformational Selection" Folding Pathways. *J. Phys. Chem. B* **2019,** *123* (9), 2005-2015.

33. Ciuba, M. A.; Levitus, M., Manganese-Induced Triplet Blinking and Photobleaching of Single Molecule Cyanine Dyes. *ChemPhysChem* **2013,** *14* (15), 3495-3502.

34. Sung, H.-L.; Nesbitt, D. J., High Pressure Single-Molecule FRET Studies of the Lysine Riboswitch: Cationic and Osmolytic Effects on Pressure Induced Denaturation. *Phys. Chem. Chem. Phys.* **2020,** *22* (28), 15853-15866.

35. Sengupta, A.; Sung, H.-L.; Nesbitt, D. J., Amino Acid Specific Effects on RNA Tertiary Interactions: Single-Molecule Kinetic and Thermodynamic Studies. *J. Phys. Chem. B* **2016,** *120* (41), 10615-10627.

36. Vieweger, M.; Holmstrom, Erik D.; Nesbitt, David J., Single-Molecule FRET Reveals Three Conformations for the TLS Domain of Brome Mosaic Virus Genome. *Biophys. J.* **2015,** *109* (12), 2625-2636.

37. Sung, H.-L.; Nesbitt, D. J., Effects of Molecular Crowders on Single-Molecule Nucleic Acid Folding: Temperature-Dependent Studies Reveal True Crowding vs Enthalpic Interactions. *J. Phys. Chem. B* **2021,** *125* (48), 13147-13157.

38. Nordmeier, E., Effects of Pressure on the Helix-Coil Transition of Calf Thymus DNA. *J. Phys. Chem.* **1992,** *96* (3), 1494-1501.

39. Wu, J. Q.; Macgregor, R. B., Jr., Pressure Dependence of the Melting Temperature of dA•dT Polymers. *Biochemistry* **1993,** *32* (46), 12531-12537.

40. Price, Ian R.; Gaballa, A.; Ding, F.; Helmann, John D.; Ke, A., Mn^{2+}-Sensing Mechanisms of *yybP-ykoY* Orphan Riboswitches. *Mol. Cell* **2015,** *57* (6), 1110-1123.

41. Serganov, A.; Nudler, E., A Decade of Riboswitches. *Cell* **2013,** *152* (1), 17-24.

42. Sung, H.-L.; Nesbitt, D. J., Novel Heat-Promoted Folding Dynamics of the *yybP-ykoY* Manganese Riboswitch: Kinetic and Thermodynamic Studies at the Single-Molecule Level. *J. Phys. Chem. B* **2019,** *123* (26), 5412-5422.

43. Mikulecky, P. J.; Feig, A. L., Cold Denaturation of the Hammerhead Ribozyme. *J. Am. Chem. Soc.* **2002,** *124* (6), 890-891.

44. Reining, A.; Nozinovic, S.; Schlepckow, K.; Buhr, F.; Fürtig, B.; Schwalbe, H., Three-State Mechanism Couples Ligand and Temperature Sensing in Riboswitches. *Nature* **2013,** *499* (7458), 355-359.

45. Chen, C. R.; Makhatadze, G. I., Molecular Determinant of the Effects of Hydrostatic Pressure on Protein Folding Stability. *Nat. Commun.* **2017,** *8* (1), 14561.

46. Heremans, K., High Pressure Effects on Proteins and other Biomolecules. *Annu. Rev. Biophys.* **1982,** *11* (Volume 11, 1982), 1-21.

47. Watson, J. D.; Crick, F. H. C., Molecular Structure of Nucleic Acids: A Structure for Deoxyribose Nucleic Acid. *Nature* **1953,** *171* (4356), 737-738.

48. Najaf-Zadeh, R.; Wu, J. Q.; Macgregor, R. B., Effect of Cations on the Volume of the Helix-Coil Transition of Poly[d(A-T)]. *BBA - Gene Struct. Expr.* **1995,** *1262* (1), 52-58.

49. Chalikian, T. V.; Macgregor, R. B., Nucleic Acid Hydration: a Volumetric Perspective. *Phys. Life Rev.* **2007,** *4* (2), 91-115.

50. Barbosa, R. d. C.; Barbosa, M. C., Hydration Shell of the TS-Kappa Protein: Higher Density Than Bulk Water. *Phys. A Stat. Mech. Appl.* **2015,** *439*, 48-58.

51. Buckin, V.; Tran, H.; Morozov, V.; Marky, L. A., Hydration Effects Accompanying the Substitution of Counterions in the Ionic Atmosphere of Poly(rA)·Poly(rU) and Poly(rA)·2Poly(rU) Helices. *J. Am. Chem. Soc.* **1996,** *118* (30), 7033-7039.

52. Knight, A. W.; Kalugin, N. G.; Coker, E.; Ilgen, A. G., Water Properties under Nano-Scale Confinement. *Sci. Rep.* **2019,** *9* (1), 8246.

53. Zhang, H.; Marko, J. F., Maxwell Relations for Single-DNA Experiments: Monitoring Protein Binding and Double-Helix Torque with Force-Extension Measurements. *Phys. Rev. E* **2008,** *77* (3), 031916.

Figures and Figure Captions

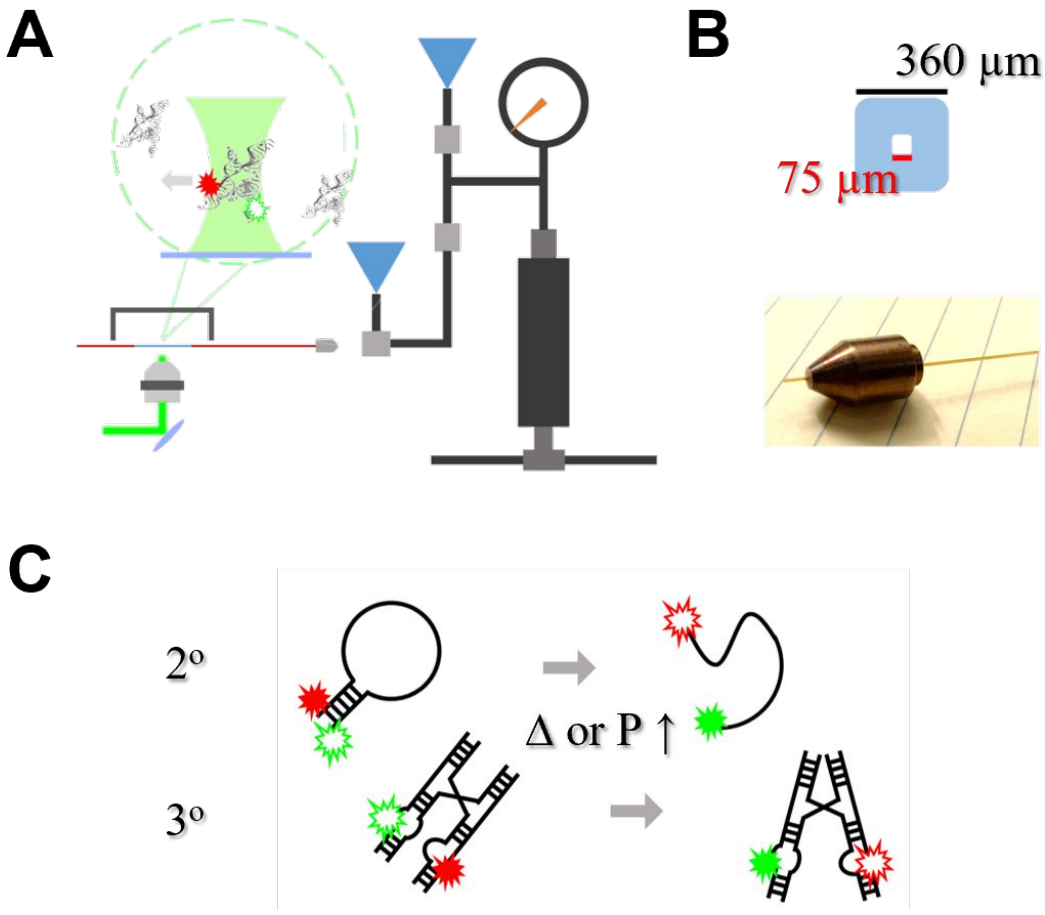

Figure 1. Schematic of the high-pressure smFRET apparatus. **A.** High pressures (up to 5 kbar) are generated by a manual piston pump and transmitted to a capillary sample holder through high-pressure stainless steel tubing. The optical window of the capillary sample holder is aligned to the microscope objective with a collar heater, with temperature fluctuations reduced and heating efficiency improved by a sample cover. **B.** The square interior capillary (75 µm x 75 µm), with a picture of the capillary glued into a pressure ferrule to couple into the high-pressure tubing. **C.** Cartoon representation of 40A DNA hairpin (secondary) and RNA Mn^{2+} riboswitch (tertiary) unfolding in response to increased heating and pressure.

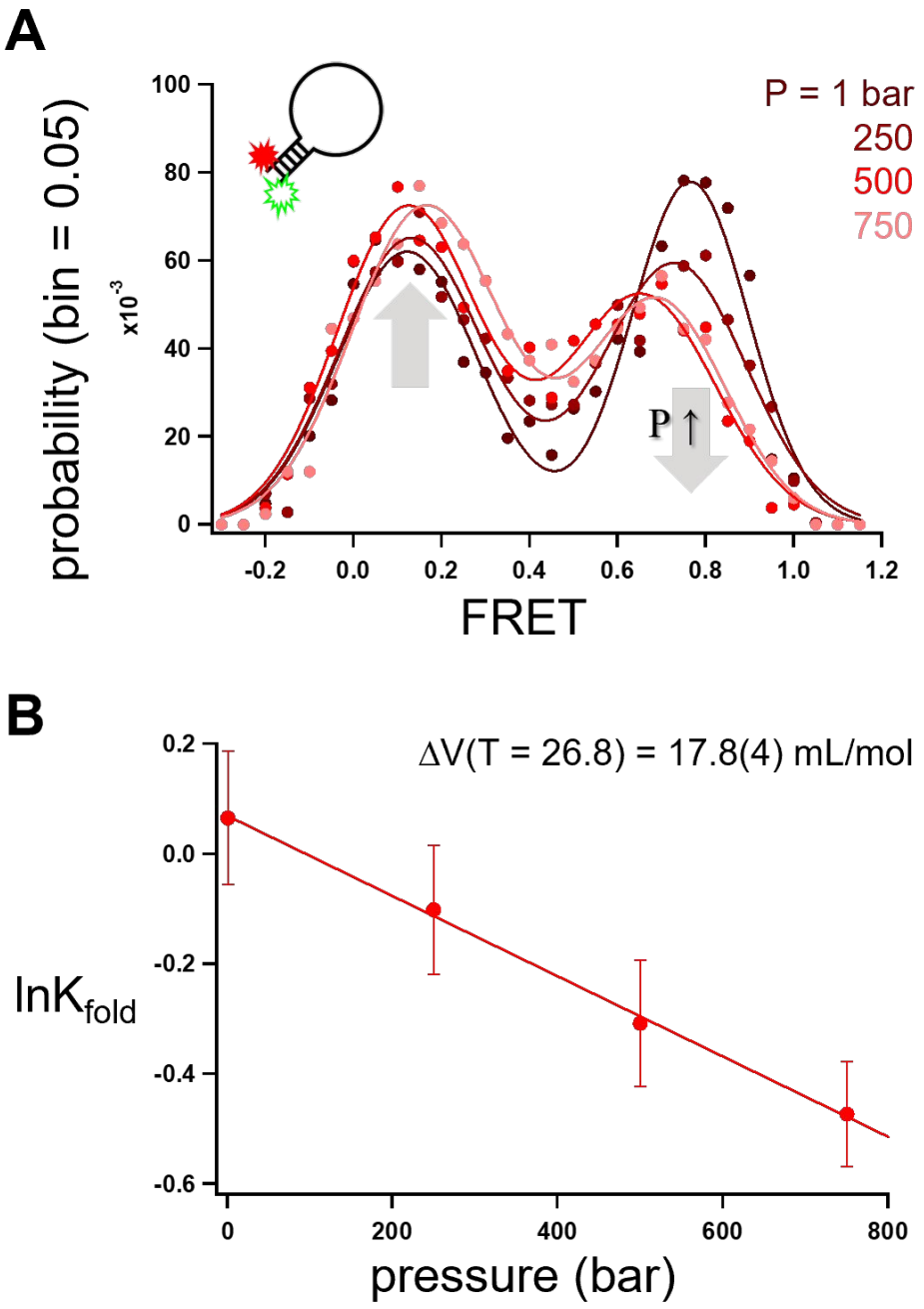

Figure 2. Sample data for pressure dependent DNA hairpin dehybridization/unfolding. **A**. Histograms of smFRET data reveal two subpopulations of the 40A DNA hairpin construct with distinct FRET values 0.2 and 0.8, corresponding to unfolded and folded states, respectively. **B.** A van't Hoff plot of $\ln K_{eq}$ vs pressure plot illustrating DNA hairpin unfolding with increasing pressure. The FRET data in A are fit to a sum of 2 Gaussians, with uncertainties in B representing error bars in the least squares analysis.

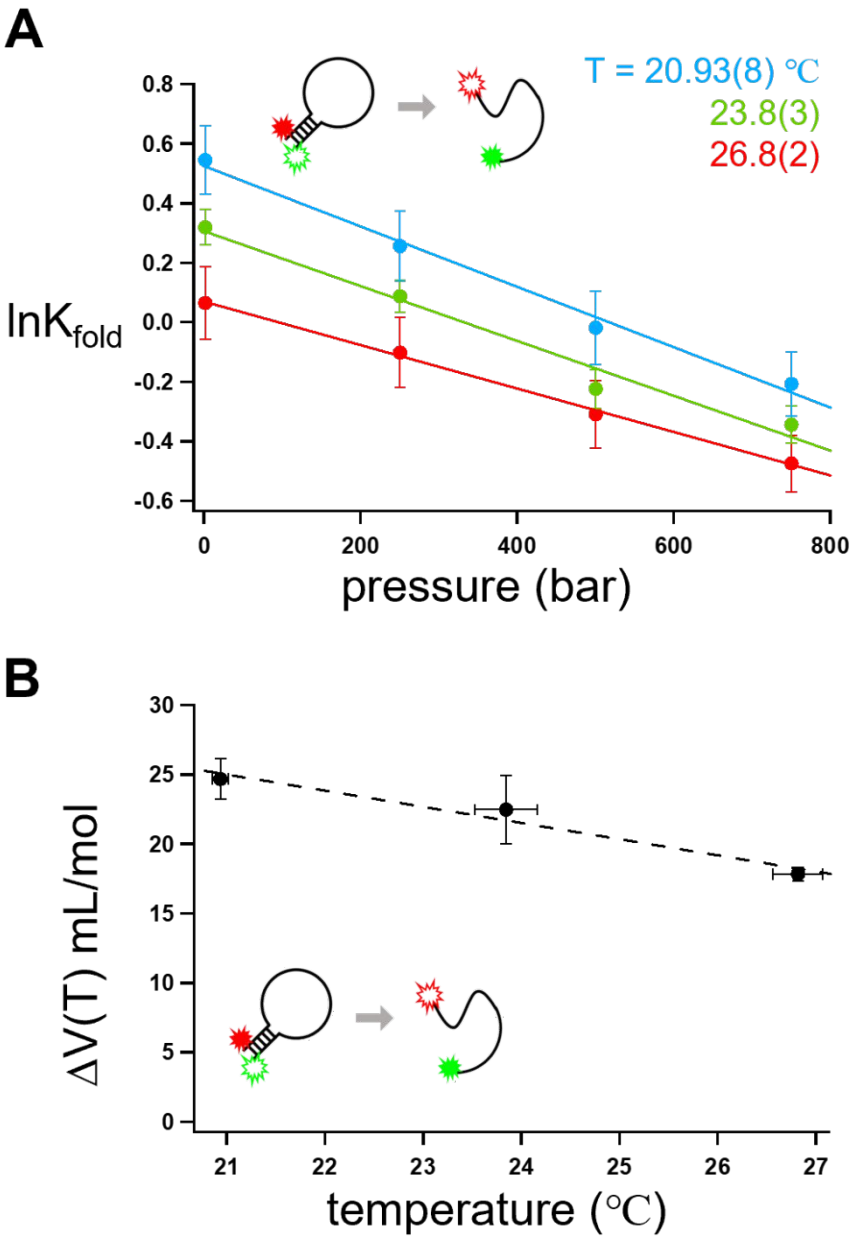

Figure 3. Temperature dependent volumetric analysis of 40A DNA hairpin hybridization. **A.** Linear least squares fits of $\ln K_{eq}$ vs pressure permit volume changes due to DNA secondary structure folding $\Delta V(T)$ to be obtained as a function of temperature. **B.** Plot of temperature dependent data $\Delta V(T)$ indicate a decrease in 40A DNA hairpin expansion volume with increasing temperature. Error bars in A represent uncertainties in the two-Gaussian E_{FRET} least squares fits. 2D error bars in B reflect least squares fit uncertainties in $\Delta V(T)$ and measured fluctuations in T.

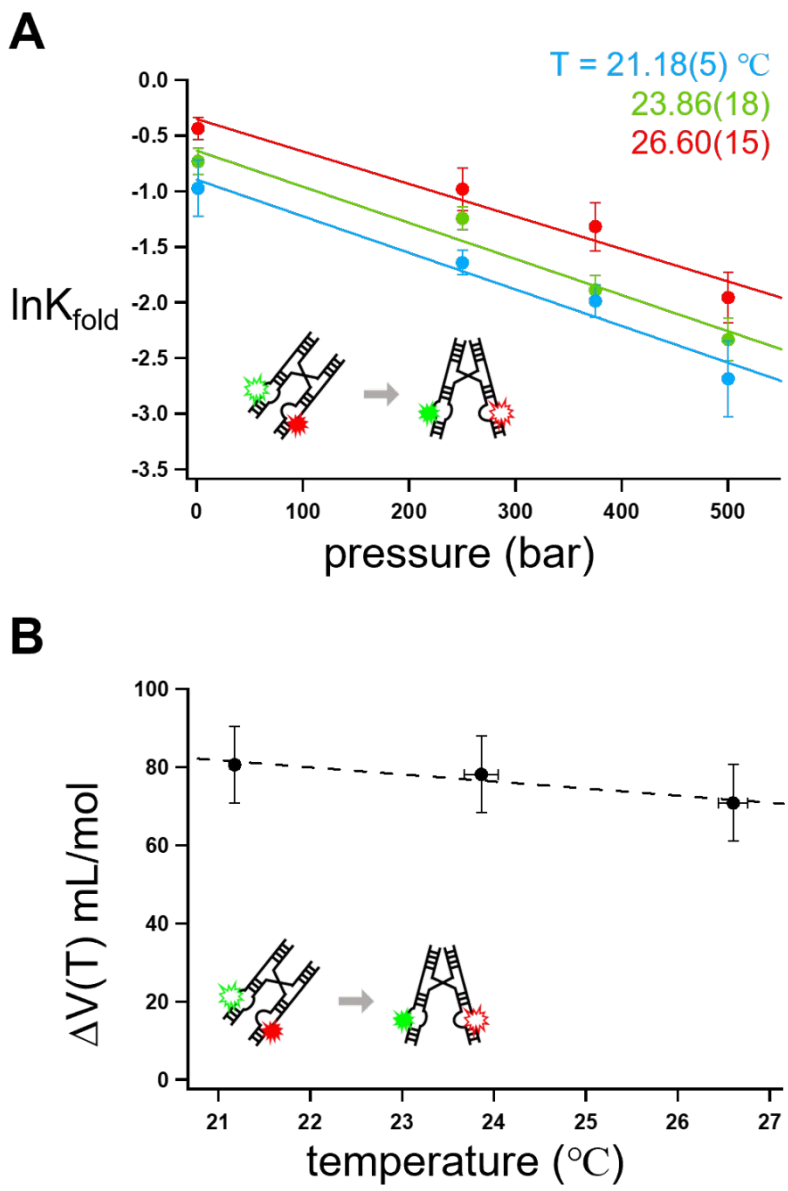

Figure 4. Temperature dependent volumetric analysis of tertiary folding for the RNA Mn^{2+} riboswitch. **A.** Van't Hoff linear fits of $\ln K_{eq}$ vs pressure permit the volume change for RNA folding $\Delta V(T)$ to be obtained as a function of temperature. **B**. Plot of $\Delta V(T)$ vs T illustrating that expansion of RNA due to tertiary folding decreases with increasing temperatures. Error bars in **A** represent uncertainties in the two-Gaussian E_{FRET} least squares fits. 2D error bars in **B** reflect least squares fit uncertainties in $\Delta V(T)$ and measured fluctuations in T.

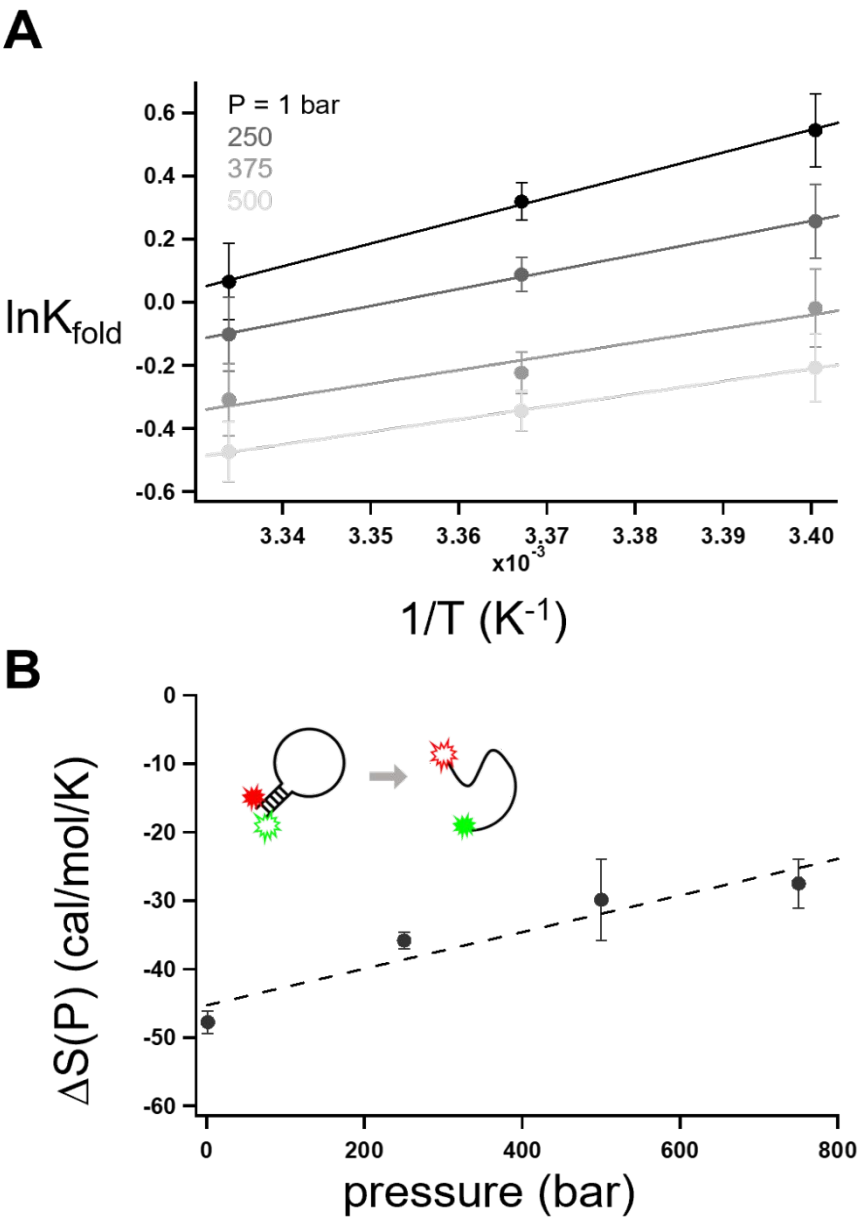

Figure 5. Temperature dependent Van 't Hoff plots for 40A DNA hairpin hybridization. **A.** Positive van't Hoff plot slopes indicate that the DNA unfolds with increasing temperature, i.e., folding of the DNA hairpin is exothermic ($\Delta H^0 < 0$). **B.** Pressure dependent entropy changes for secondary structure formation ($\Delta S(P)$) obtained from the intercepts in **A** indicating a systematic *decrease* in entropic penalty ($\Delta\Delta S > 0$) with pressure. Error bars in **A** and **B** represent uncertainties from least squares fits to a linear function

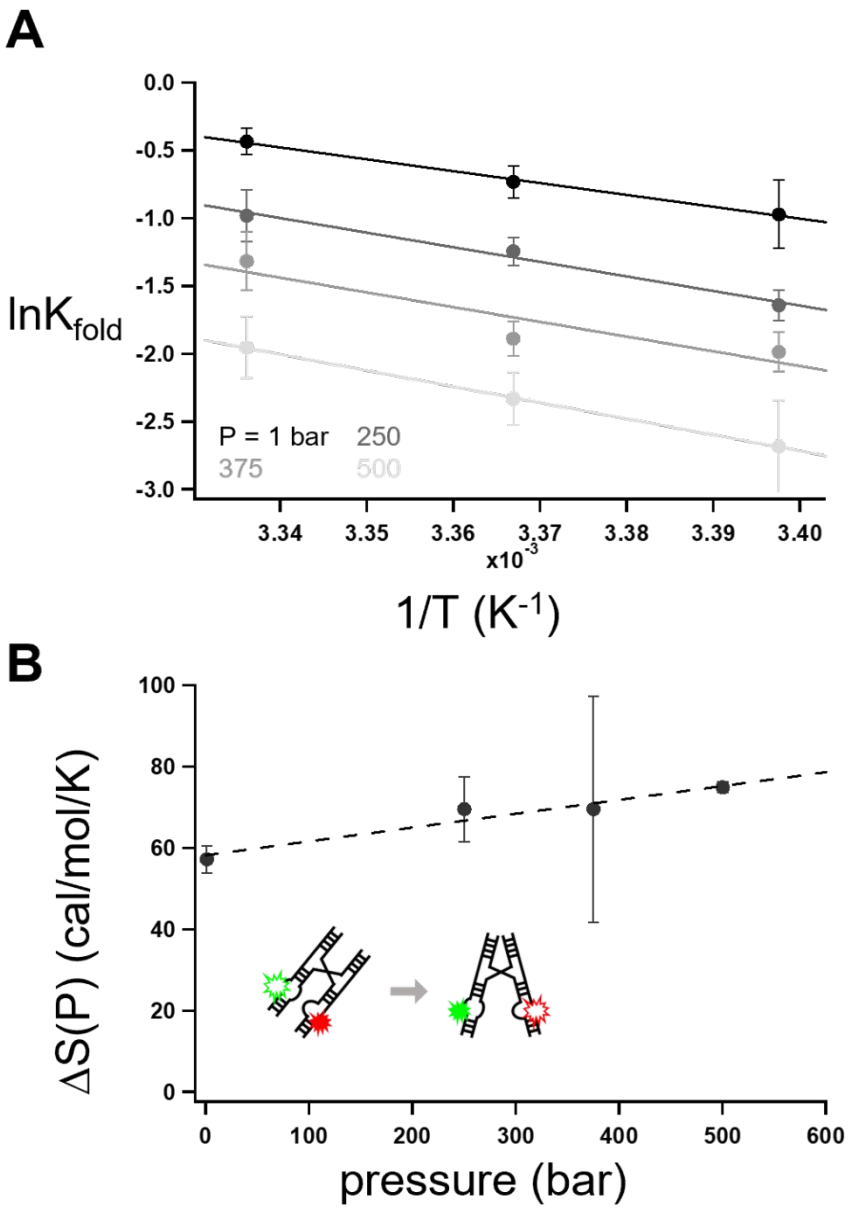

Figure 6. Pressure/temperature dependent tertiary folding of the RNA Mn^{2+} riboswitch. **A.** The negative slopes in the van't Hoff plots indicate novel heat induced folding with *increasing* temperatures, which implies tertiary folding to be *endothermic* ($\Delta H^0 > 0$). **B.** Data revealing the corresponding folding entropies ($\Delta S(P)$) for tertiary structure formation in the RNA riboswitch increase as a function of increasing pressure, despite the unconventional positive ΔH^0. Error bars in A and B reflect least square uncertainties in the two-Gaussian E_{FRET} distributions and the van't Hoff intercepts ($\Delta S(P)$), respectively.

40A DNA Hairpin ΔV(T)	
Temperature (°C)	ΔV(mL/mol)
20.93(8)	24.7(14)
23.8(3)	22(2)
26.8(2)	17.9(4)

Table 1. Temperature dependent volume changes ΔV(T) due to secondary structure folding of the 40A DNA hairpin construct obtained from linear fits in Fig. 3A. Uncertainties reflect 1σ least squares fitting errors in ΔV and measured fluctuations in T.

Mn^{+2} Riboswitch ΔV(T)	
Temperature (°C)	ΔV (mL/mol)
21.18(5)	81(9)
23.86(18)	78(9)
26.6(15)	71(9)

Table 2. Temperature dependent volume changes ΔV(T) due to tertiary structure folding of the RNA Mn^{2+} riboswitch obtained from linear fits in Fig. 4A. Uncertainties reflect 1σ least squares fitting errors in ΔV and measured fluctuations in T.

40A DNA Hairpin

P(bar)	ΔS (cal/mol/K)	ΔH (kcal/mol)	α (mL/mol/K)
1	-47.7(15)	-14.35(16)	
250	-35.8(11)	-10.71(14)	
500	-30(5)	-8.7(18)	
750	-27(3)	-8.0(9)	
			-1.16(23)

Table 3. Pressure dependent entropy/enthalpy changes ΔS(P)/ΔH(P) for folding of the 40A DNA hairpin construct obtained from linear fits in Fig. 5A. Uncertainties reflect 1σ least squares fitting errors in ΔV.

Mn^{+2} Riboswitch

P(bar)	ΔS (cal/mol/K)	ΔH (kcal/mol)	α (mL/mol/K)
1	57(3)	17.4(10)	
250	70(7)	21(2)	
375	70(27)	22(8)	
500	75(13)	23.6(4)	
			-1.8(5)

Table 4. Pressure dependent entropy/enthalpy changes ΔS(P)/ΔH(P) for tertiary folding of the RNA Mn^{2+} riboswitch construct obtained from linear fits in Fig. 6A. Uncertainties reflect 1σ least squares fitting errors in ΔV.

Testing Maxwell's Relations at the Single Molecule Level	
40A DNA hairpin	
$(\partial\Delta S/\partial P)_T$	$-(\partial\Delta V/\partial T)_P$
1.11(25) mL/mol/K	1.16(23) mL/mol/K
Mn^{+2} Riboswitch	
$(\partial\Delta S/\partial P)_T$	$-(\partial\Delta V/\partial T)_P$
1.40(24) mL/mol/K	1.8(5) mL/mol/K

Table 5. Novel tests of the thermodynamic Maxwell relation at the single molecule level. Agreement with $(\partial\Delta S/\partial P)_T = -(\partial\Delta V/\partial T)_P$ is well within the reported (1σ) error bars for both the 40A DNA hairpin secondary structure formation and tertiary folding of the RNA Mn^{2+} riboswitch.

All graphical data for this article will be made available at Open Science Framework, with a link provided to PPCP prior to publication